Local structure and dynamics in relaxor-ferroelectric $PbSc_{1/2}Nb_{1/2}O_3$ and $PbSc_{1/2}Ta_{1/2}O_3$ single crystals

2002 J. Phys.: Condens. Matter 14 1091

(http://iopscience.iop.org/0953-8984/14/5/314)

INSTITUTE OF PHYSICS PUBLISHING JOURNAL OF PHYSICS: CONDENSED MATTER

J. Phys.: Condens. Matter **14** (2002) 1091–1105 PII: S0953-8984(02)29275-9

Local structure and dynamics in relaxor-ferroelectric $PbSc_{1/2}Nb_{1/2}O_3$ and $PbSc_{1/2}Ta_{1/2}O_3$ single crystals

B Mihailova[1,2], U Bismayer[1], B Güttler[3], M Gospodinov[4] and L Konstantinov[2]

[1] Mineralogisch-Petrographisches Institut, Universität Hamburg, Grindelallee 48, 20146 Hamburg, Germany
[2] Central Laboratory of Mineralogy and Crystallography, Bulgarian Academy of Sciences, Acad. G. Bonchev Street, Building 107, 1113 Sofia, Bulgaria
[3] Physikalisch-Technische Bundesanstalt, Bundesallee 100, 38116 Braunschweig, Germany
[4] Institute of Solid State Physics, Bulgarian Academy of Sciences, Blvd Tzarigradsko Chausse 72, 1784 Sofia, Bulgaria

E-mail: mi0a007@uni-hamburg.de (B Mihailova)

Received 28 September 2001, in final form 13 December 2001
Published 25 January 2002
Online at stacks.iop.org/JPhysCM/14/1091

Abstract

Local structural arrangements and corresponding dynamical effects in relaxor ferroelectrics $PbSc_{1/2}Nb_{1/2}O_3$ and $PbSc_{1/2}Ta_{1/2}O_3$ were studied by Raman spectroscopy. Polarized Raman spectra of single crystals were measured at different temperatures in several scattering configurations. The peaks observed are assigned on the basis of normal-mode calculations. The effect of small structural deviations on the atomic vibrations is analysed by calculating the modes of structural units at various atomic positions. It is shown that doubling the structural unit is always possible on a local scale of a few unit cells. The presence of two Raman peaks originating from the F_{2u} mode shows that electron–phonon coupling occurs in $PbSc_{1/2}B''_{1/2}O_3$, thus leading to dynamical off-centre-symmetrical structural fluctuations. The structural perturbation consists of the non-coplanarity of Pb and O atoms in the planes perpendicular to the body diagonal and deviations of B cations from the centre of BO_6 octahedra. The intensity ratio of the two peaks is sensitive to the degree of orientational ordering of the lone pairs of Pb atoms within the Pb–O planes, which is related to the degree of compositional B′/B″ ordering. The temperature dependence of the peaks arising from asymmetrical O–B–O bending, BO_3 translation and Pb-localized modes shows that on cooling different structural changes are preferential in the two materials studied. In $PbSc_{1/2}Nb_{1/2}O_3$ the lowering of the temperature favours the off-centre deviations of the B cations. In $PbSc_{1/2}Ta_{1/2}O_3$ the temperature decrease stabilizes the non-coplanarity of the Pb and O atoms in the planes perpendicular to the body diagonal and enhances the correlation between the electronic lone pairs of Pb.

1. Introduction

Relaxors form a special class of ferroelectrics which are characterized by a broad diffuse phase transition near the dielectric constant maximum, frequency dependence of $\varepsilon(T)$ and a high magnitude of permittivity in the Curie range. Such properties make relaxor materials very attractive for practical application in various ferroelectric-related devices [1]. They are also interesting from a fundamental point of view, since the true origin of the diffuse phase transition is still controversial and the question of the local structure and its influence on the macroscopic properties is still open.

Most of the relaxors are lead-based perovskite-type compounds with general formula $Pb(B', B'')O_3$, $B' = Fe^{2+}, Mg^{2+}, Ni^{2+}, Zn^{2+}, In^{3+}, Sc^{3+}$; $B'' = Nb^{5+}, Ta^{5+}, W^{6+}$. Their structure has extensively been studied by different experimental methods: x-ray and neutron diffraction [2–7], x-ray diffuse scattering [8], infrared and Raman spectroscopy [9–17], nuclear magnetic resonance [18], high-resolution transmission electron microscopy [19–21] and scanning force microscopy [22]. The relaxor behaviour is closely related to the short-range order of the sublattice sites and the existence of domains ranging in size from several angstroms up to hundreds of nanometres. The effect of the compositional B′/B″ ordering, which depends on the preparation procedure and which can be changed by subsequent annealing, has been previously discussed [5, 23–27]. The affinity to B-site ordering is generally determined from the valence and the ionic radii differences between B′ and B″ cations. The chemical stoichiometry of $PbSc_{1/2}Nb_{1/2}O_3$ (PSN) and $PbSc_{1/2}Ta_{1/2}O_3$ (PST) facilitates the formation of ordered domains and the degree of the chemical order in these compounds can easily be controlled by thermal treatment [28]. However, Ta and Sc atoms show a tendency to order easier than Nb and Sc atoms, although the ionic radii of Ta^{5+} and Nb^{5+} in a six-coordination are the same, $r_{Ta} = r_{Nb} = 0.64$ Å [29]. Another interesting point is that in PST the chemical order shifts the permittivity maximum to a higher temperature, while in PSN the chemical order shifts the permittivity maximum to a lower temperature [5, 23]. In addition, the dielectric constant of chemically disordered ceramic samples differs from that of chemically disordered single crystals. Obviously, the relaxor properties depend also on different types of structural disorder existing on the intermediate-range scale. Hard-mode spectroscopy, which has been applied to PST, revealed the complex atomic arrangement in this material [11]. A number of peaks, more than those predicted by group theory, have been observed for both ordered and disordered crystals. Additionally, the temperature dependence of the peak widths suggests the presence of precursor clusters in the Curie range. Although the exact origin of the Raman peaks has not been specified until now, it is clear that within several unit cells, which is the sensitivity of the Raman spectroscopy, the relaxor structure is different from the average structure detected by diffraction methods. High-resolution transmission electron microscopy and x-ray diffuse scattering give some insights about local atomic deviations from the ideal perovskite positions, but predominantly for the heavy cations. Raman spectroscopic investigations on various relaxors have shown that, irrespective of the chemical stoichiometry of B-cations, near the permittivity maximum temperature the symmetry of the nanosized regions is face-centred cubic, which is typical of 1:1 B-site ordered systems [16]. However, the dynamic state of the nanoscaled structural aggregates is still not clarified.

This paper aims to compare temperature-dependent polarized Raman spectra of two relaxors with equal stoichiometry, PSN and PST, and, on this basis, to assign the observed Raman scattering to definite atomic vibrations and to gain further information on the atomic arrangement near the Curie regime in relaxors.

2. Experimental details

Single crystals of PSN and PST were synthesized by the high-temperature solution growth method. Cubic-shaped samples with typical size of 3 mm were grown in a PbO + PbF_2 + B_2O_3 flux by slow cooling. The as-synthesized crystals were characterized by electron microprobe analysis (Camebax microbeam SEM-system), powder x-ray diffraction (XRD) analysis (Philips X'Pert diffractometer) and single-crystal x-ray diffraction analysis (Nonius Kappa CCD diffractometer). The Raman measurements were performed using a triple monochromator system (Jobin-Yvon T64000) equipped with an Olympus BH2 microscope. The spectra were collected in back-scattering geometry using the 514.5 nm line of an Ar^+ laser and a laser beam power of 10 mW on the sample surface. The spectral resolution achieved was about 2 cm^{-1}. Parallel (p) and cross (c) polarized spectra were recorded at four different temperatures: 160, 220, 290 and 410 K and in two different experimental geometries: (i) when the polarization of the incident light was parallel to the cubic edge and (ii) when the polarization of the incident light was parallel to the cubic face diagonal. We did not detect any dependence of the spectra data on the localization of the laser spot on the sample surface as well as on the spot diameter, being varied between 1.2 and 6 μm. The measured spectra were temperature-corrected for the Bose–Einstein phonon occupation factor and smoothed by the adjacent averaging method.

3. Results and discussion

The structure of the para- and ferro-electric phase of PSN has been refined by neutron diffraction [4–6]. The symmetry of the paraelectric disordered PSN has been determined as cubic, $Pm\bar{3}m$, and that of the ferroelectric phase as rhombohedral, $R3m$, with a weak angle distortion ($\alpha_r \approx 89.87^\circ$ at 2 K) and small atomic displacements along the cubic body diagonal. The phase transition temperature has been reported to be between 375 and 400 K in disordered PSN and at 351 K in ordered PSN. Disordered PST undergoes para-to-ferro phase transition around 270 K and the space group is changed from $Pm\bar{3}m$ to $R3m$ or $R3$ [2]. The phase transition of PST with a high degree of compositional order is just above room temperature and the structure of the paraelectric phase has been refined in the $Fm\bar{3}m$ space group [7]. The exact space group of the low-temperature modification of PST has not yet been determined [21,30]. Hysteresis and dielectric measurements on PST films reveal the existence of additional phase transitions at 233, 160 and 50 K [31]. The electric anomalies at 233 K have been interpreted as due to a rhombohedral-to-monoclinic transition. The peculiarities at 160 and 50 K have been supposed to possibly arise from a monoclinic-to-triclinic transition and from unit cell multiplication, respectively.

We performed XRD measurements on our samples at room temperature. According to the powder XRD data both PSN and PST are chemically disordered as no doubling of the unit cell could be observed. The single-crystal diffraction data also pointed to the lack of any compositional ordering in PSN and the structure was considered as pseudo-cubic with unit cell parameter $a = 4.0872$ Å. However, in PST weak superlattice reflections were detected by the single-crystal diffraction technique, thus giving evidence for the presence of weak B′/B″ ordering. The structure could be refined in $Fm\bar{3}m$ symmetry with $a = 8.1645$ Å and Pb, Sc/Ta and O atoms in 8*c*, 4*a*/4*b* and 24*e* Wyckoff positions, respectively.

The vibrational modes predicted by the group theory analysis [32] for chemically disordered and ordered $PbSc_{1/2}B''_{1/2}O_3$ crystals, when $R3m$ space group is assumed for the ferroelectric phase, are given in table 1. In case of $R3$ symmetry the number of the optical modes will be unchanged, but all A-modes become simultaneously Raman and infrared active.

Table 1. Normal modes in $PbSc_{1/2}B''_{1/2}O_3$ crystals according to group theory analysis. ir, infrared-active; r, Raman-active; ina, inactive.

	B′/B″ disordered, $Z = 1$		B′/B″ ordered, $Z = 2$	
	para, $Pm\bar{3}m$	ferro, $R3m$	para, $Fm\bar{3}m$	ferro, $R3m$
Pb	F_{1u}	$A_1 + E$	$F_{1u} + F_{2g}$	$2A_1 + 2E$
Sc, B″	F_{1u}	$A_1 + E$	F_{1u} F_{1u}	$A_1 + E$ $A_1 + E$
O	$2F_{1u} + F_{2u}$	$2A_1 + A_2 + 3E$	$A_{1g} + E + F_{1g} + 2F_{1u} + F_{2g} + F_{2u}$	$4A_1 + 2A_2 + 6E$
Phonon activity and correlation			A_{1g}(r) E_g(r) F_{1g}(ina)	A_1(r, ir) E(r, ir) A_2(ina) + E(r, ir)
	F_{1u} (ir)	A_1(r, ir) + E (r, ir)	F_{1u} (ir)	A_1(r, ir) + E (r, ir)
			F_{2g}(r)	A_1(r, ir) + E (r, ir)
	F_{2u} (ina)	A_2(ina) + E(r, ir)	F_{2u} (ina)	A_2(ina) + E(r, ir)
Optical phonons	$3F_{1u} + F_{2u}$	$3A_1 + A_2 + 4E$	$A_{1g} + E_g + F_{1g} + 4F_{1u} + 2F_{2g} + F_{2u}$	$7A_1 + 2A_2 + 9E$
Raman active	—	$3A_1 + 4E$	$A_{1g} + E_g + 2F_{2g}$	$7A_1 + 9E$

The intensity of the Raman scattering from a mode of a certain symmetry depends on the polarization geometry. Table 2 presents the polarizabilty tensors of the Raman-active modes in a cubic system for the two geometries used in our experiments. As can be seen, if the incident light polarization e_i is along the cubic edge, the A- and E-modes of the paraphase will appear in the p-polarized spectrum, while the F-modes will be observed in the c-polarized spectrum. Hence, if e_i is parallel to the cubic face diagonal, all A-, E- and F-modes will contribute to the p-polarized spectrum, while the c-polarized spectrum will be determined from the E- and F-modes. The contribution of the A- and E-modes of the rhombohedral ferroelectric phase to the spectra of different polarization is more complicated, since the light does not propagate along a crystallographic direction of the trigonal system. Additionally, depolarization effects due to the existence of ferroic domains are expected. Thus the A- and E-modes of the ferrophase may be observed in all the polarization geometries used. Correct normal-mode determination for the supposed monoclinic low-temperature phase is hampered by insufficiency of precise structural data. Generally, if the rhombohedral-to-monoclinic phase transition takes place, there would be a larger number of Raman peaks than expected for the rhombohedral phase due to the splitting of the 'rhombohedral' doubly-degenerated modes' to 'monoclinic' single modes.

The measured Raman spectra of PSN are shown in figure 1 and those of PST in figure 2. The spectra collected at different temperatures were normalized to each other using the height of the peak near 820 cm^{-1} in the p-polarization. The positions of the peaks observed in the spectra of PSN and PST are listed in tables 3 and 4, respectively. Several spectral features were observed as follows.

Both materials produce Raman scattering strongly dependent on the polarization geometry. The Raman spectra of PSN and PST are similar and at higher temperatures the same number of peaks is observed. The spectra differ mainly in the intensity ratios between some peaks, especially that between the peaks near 350 and 300 cm^{-1}. The peak positions in the spectra of the two materials are found to be different. One can separate two groups of peaks: (i) P_1, P_2, P_5, P_7 and P_8 which appear at lower frequencies in the spectra of PSN than in the spectra of PST and (ii) P_4, P_6, P_9 and P_{10} whose frequencies are higher in the spectra of PSN than in the

Table 2. Polarizability tensors of Raman-active modes in a cubic system.

	Light propagation along [001], e_i along [010]	Light propagation along [001], e_i along [110]
A	$\begin{bmatrix} a & 0 & 0 \\ 0 & a & 0 \\ 0 & 0 & a \end{bmatrix}$	$\begin{bmatrix} a & 0 & 0 \\ 0 & a & 0 \\ 0 & 0 & a \end{bmatrix}$
E	$\begin{bmatrix} b & 0 & 0 \\ 0 & b & 0 \\ 0 & 0 & -2b \end{bmatrix}$	$\begin{bmatrix} b & 0 & 0 \\ 0 & b & 0 \\ 0 & 0 & -2b \end{bmatrix}$
	$\begin{bmatrix} -\sqrt{3}b & 0 & 0 \\ 0 & \sqrt{3}b & 0 \\ 0 & 0 & 0 \end{bmatrix}$	$\begin{bmatrix} 0 & \sqrt{3}b & 0 \\ \sqrt{3}b & 0 & 0 \\ 0 & 0 & 0 \end{bmatrix}$
F	$\begin{bmatrix} 0 & 0 & 0 \\ 0 & 0 & d \\ 0 & d & 0 \end{bmatrix}$	$\begin{bmatrix} 0 & 0 & d/\sqrt{2} \\ 0 & 0 & d/\sqrt{2} \\ d/\sqrt{2} & d/\sqrt{2} & 0 \end{bmatrix}$
	$\begin{bmatrix} 0 & 0 & d \\ 0 & 0 & 0 \\ d & 0 & 0 \end{bmatrix}$	$\begin{bmatrix} 0 & 0 & d/\sqrt{2} \\ 0 & 0 & -d/\sqrt{2} \\ d/\sqrt{2} & -d/\sqrt{2} & 0 \end{bmatrix}$
	$\begin{bmatrix} 0 & d & 0 \\ d & 0 & 0 \\ 0 & 0 & 0 \end{bmatrix}$	$\begin{bmatrix} d & 0 & 0 \\ 0 & -d & 0 \\ 0 & 0 & 0 \end{bmatrix}$

Table 3. Positions of the peaks observed in the Raman spectra of $PbSc_{1/2}Nb_{1/2}O_3$. $e_i \parallel$ edge; sh, shoulder; vw, very weak.

	p-polarization				c-polarization			
	410 K	290 K	220 K	160 K	410 K	290 K	220 K	160 K
P_1	810	812	816	818	—	—	—	818
P_2	796 sh	796 sh	796 sh	796 sh	—	—	—	796 sh
P_3	700 vw	700 vw	700 vw	700 vw	—	—	—	—
P_4	610 vw	610	615	615	—	—	—	620 vw
P_5	525	530, 505 sh	530, 505 sh	530, 505 sh	525	530, 505 sh	535, 505 sh	535, 505 sh
P_6	440 vw	440 vw	440 vw	440 vw	—	440 vw	440 vw	440 vw
P_7	350 vw	350 vw	350 vw	355 vw	350	350	350	355
P_8	290 vw	290 vw	290 vw	290 vw	290	290	290	290
P_9	260	265	270	270	260	265	270	270
P_{10}	152	157	164	168	—	—	—	—
P_{11}	50	52	56	56	50	52	56	56

spectra of PST. Since the mass of Ta is larger than that of Nb, it is obvious that the latter peaks are generated from modes involving motion of B atoms, while the former peaks arise from modes without participation of B atoms. It has been shown that there is a slight increase in the covalency from niobates to tantalates in the same structure [33]. Therefore, the frequency difference of the peaks from the first group is due to different values of the interatomic force constants in PSN and PST. The weak, broad peak P_3 centred for both materials near 700 cm^{-1} could belong to the second group, but the mass effect is compensated by the force constant effect. The lowest frequency peak P_{11} is also positioned near the same frequency for both materials, most probably because it is localized in the Pb atoms.

At 410 K both materials should be in the paraelectric state. Therefore, when e_i is along the cubic edge two peaks must exist in the p-polarized spectrum of PST and no peaks for PSN

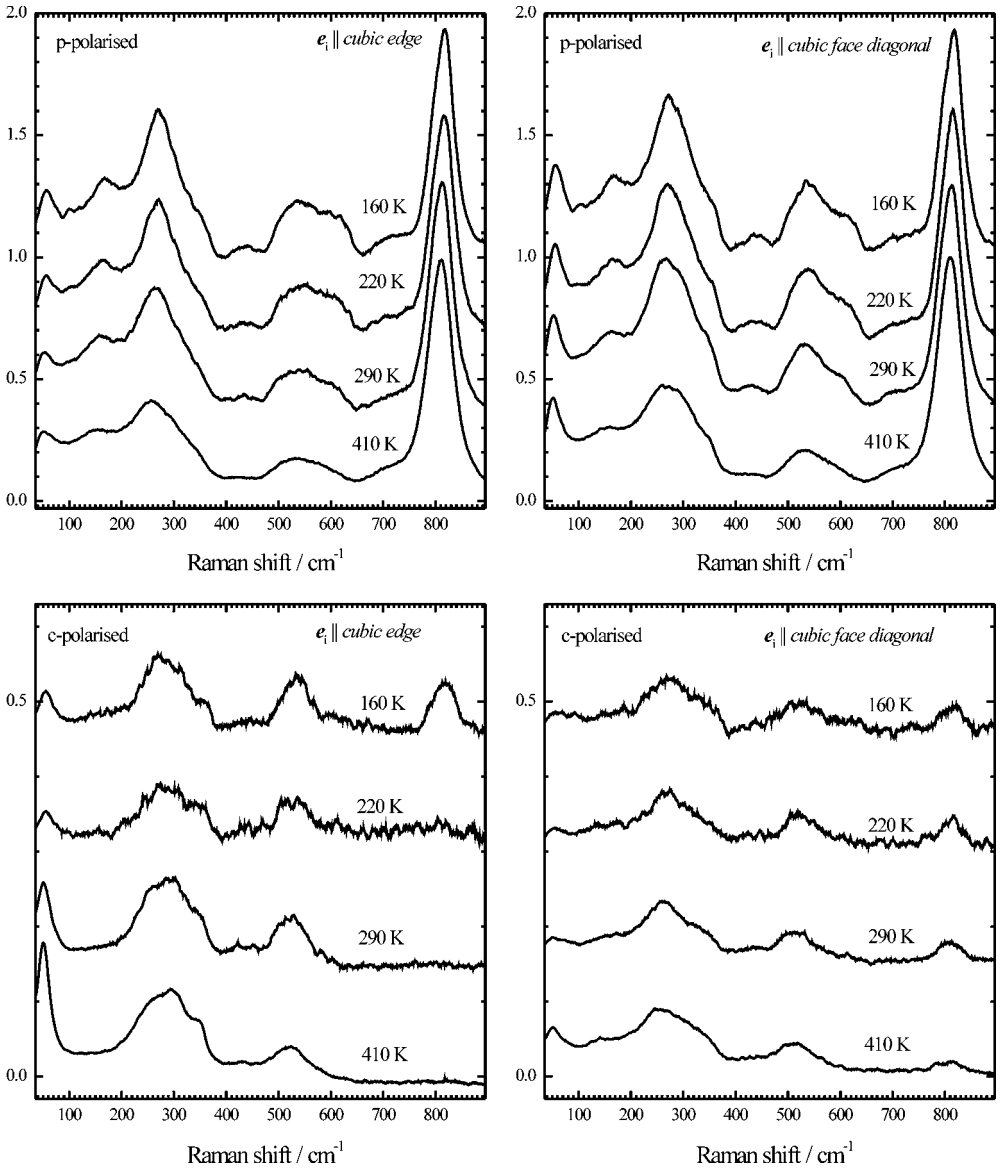

Figure 1. Reduced parallel (p) and cross (c) polarized spectra of PSN measured in different experimental orientations; e_i stands for the polarization direction of the incident light.

are expected, which strongly contradicts our observations. However, the perfect polarization of the band near 820 cm^{-1} shows unambiguously that this band results from 'cubic' A- and/or E-mode. Hence, P_2 appears in the cross polarized spectrum measured with e_i along the face diagonal, i.e. it behaves as a 'cubic' E-mode. Therefore, it is reasonable to assume that P_1 arises from the A_g-mode and P_2 from the E_g-mode, which implies a doubling of the unit cell for both materials, regardless of the degree of chemical ordering determined by XRD. In the cross polarized spectrum with e_i along the cubic edge five peaks, P_5, P_7, P_8, P_9 and P_{11}, are observed for both materials, instead of two peaks for PST and zero peaks for PSN. All five peaks are also

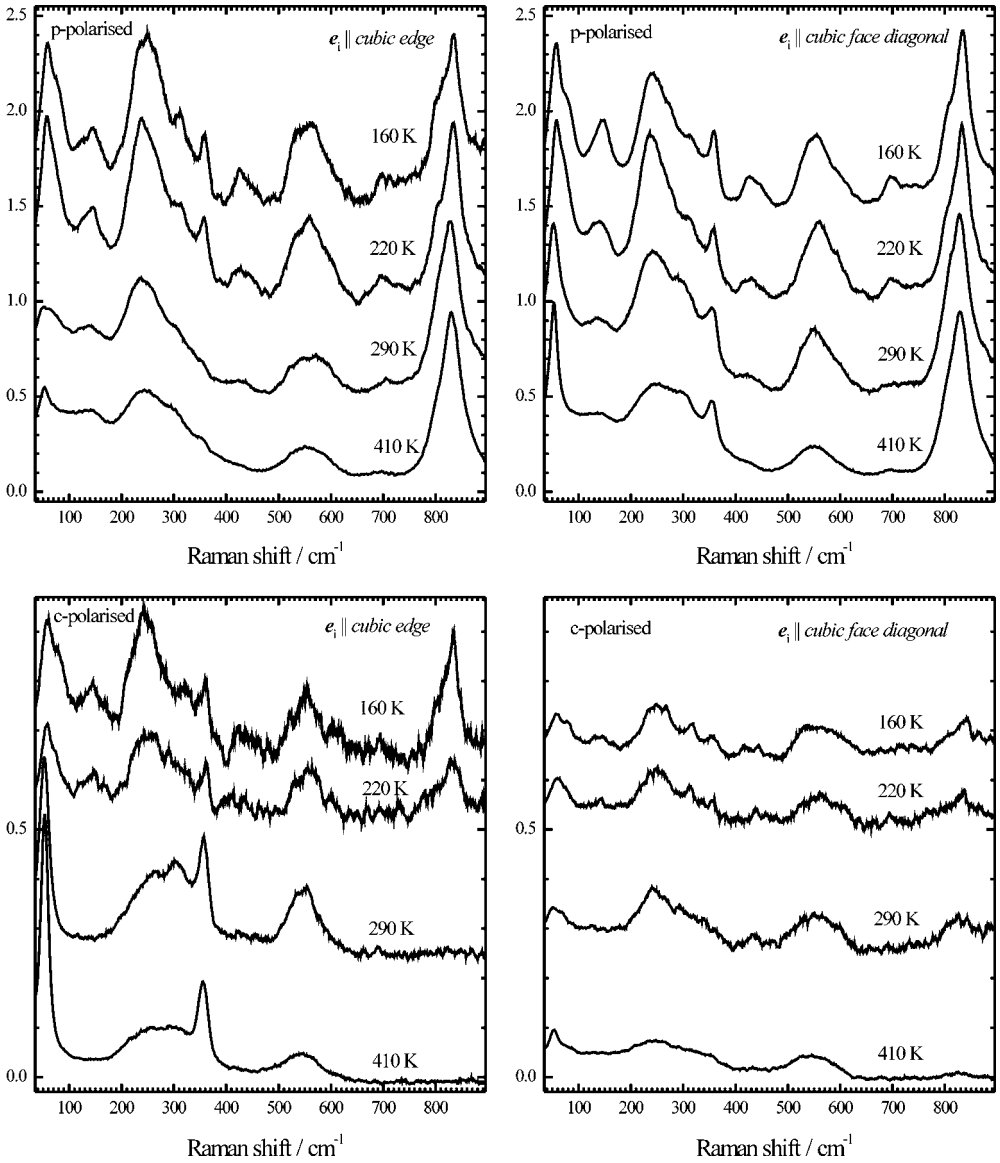

Figure 2. Reduced parallel (p) and cross (c) polarized spectra of PST measured in different experimental orientations; e_i stands for the polarization direction of the incident light.

seen in the p-polarized spectra, but the spectral profile of the depolarization ratio (figure 3) reveals that at least P_5, P_7, P_8 and P_{11} are of F-type symmetry. The stronger p-polarized Raman scattering for e_i parallel to the face diagonal compared to e_i parallel to the edge also shows that P_5, P_7, P_8 and P_{11} can be assigned as Raman-active F-modes in a cubic system. It is seen that P_7 and P_8 are related to the compositional order in the B positions. In cross-polarization with e_i parallel to the edge the intensity ratio between P_7 and P_8 is much larger for PST than for PSN and the ratios do not change substantially as the temperature decreases. This corresponds well to the single-crystal diffraction data showing the presence and absence of the B-site superlattice in PST and PSN, respectively.

Table 4. Positions of the peaks observed in the Raman spectra of $PbSc_{1/2}Ta_{1/2}O_3$. $e_i\|$ edge; sh, shoulder; w, weak.

	p-polarization				c-polarization			
	410 K	290 K	220 K	160 K	410 K	290 K	220 K	160 K
P_1	829	828	833	834	—	—	833	834
P_2	805 sh	805 sh	805 sh	805 sh	—	—	805 sh	805 sh
P_3	700 w	700 w	700 w	700 w	—	—	—	700 w
P_4	570 sh	570 sh	570 sh	570 sh	—	—	—	—
P_5	550	558, 534 sh	558, 534 sh	558, 534 sh	550	558, 534 sh	558, 534 sh	558, 534 sh
P_6	426 w	426 w	426	426	—	—	426 w	426
P_7	356 w	357 w	358	359	356	357	358	359
P_8	300 w	305 w	315	315	300	305	315	315
P_9	245	250 sh, 240	250 sh, 240	260 sh, 250 240	240–260	240–260	240–260 220 sh	260 sh 240 220 sh
P_{10}	146	146 123 sh	146, 123 sh	146, 123 sh	—	—	146, 123 sh	146, 123 sh
P_{11}	53	70 sh, 51	75 sh, 57	80 sh, 59	53	53	75 sh, 57	80 sh, 59

The weak peaks P_3, P_4, P_6 and P_{10} observed in p-polarization with e_i parallel to the edge become more pronounced when the temperature is lowered, obviously due to an increase in the ferroic structural distortion. There are some notable differences between the two materials in their temperature dependence of the scattering intensities. In the case of PST the band P_9 is resolved in several components at lower temperatures, which is not detected for PSN. This may be due to the lower symmetry of the PST ferrophase compared to that of PSN. However, one can hardly conclude whether this is a monoclinic feature or just an occurrence of $R3$ symmetry instead of $R3m$. Another distinction is that for PST the intensity of P_6 increases at a greater rate as the temperature decreases than does the intensity of P_4, while for PSN the opposite effect is observed. In addition, a high-frequency shoulder of P_{11}, whose intensity increases on cooling, is observed for PST, but not for PSN. On the other hand, cooling the sample leads to a frequency increase of the P_{10} peak in the p-polarized spectrum of PSN, but does not affect the frequency of the same peak in the spectrum of PST. Thus, the temperature dependence of the spectra reveals that different phenomena occur in the two compounds during the phase transition.

To better understand the observed spectral peculiarities we performed normal-mode calculations for a pseudo-cubic perovskite structure of the $PbB'_{1/1}B''_{1/2}O_3$ type. The force constant method used is described in details elsewhere [34, 35]. Briefly, in this approach the eigenfrequencies and the atomic vector displacements are found through diagonalizing the dynamical matrix of a representative structural unit with imposed boundary conditions. The dynamical matrix elements are calculated from the atomic Cartesian coordinates and force constants accounting for different types of interaction. The induced dipole moment and the polarizability tensor are calculated from the vector displacements, charges, polarizabilities and electronegativities of the atoms [36–38]. The method is not restricted by any symmetry constrains in the computing procedure and is useful in following the dependence of the frequencies and relative intensities on local structural changes.

In this study we consider three types of interatomic interactions: (i) a bond stretching, between two atoms forming a bond; (ii) a bond bending, between three atoms forming a bond angle, and (iii) a Coulomb-type interaction, between two non-bonded atoms. We concentrated

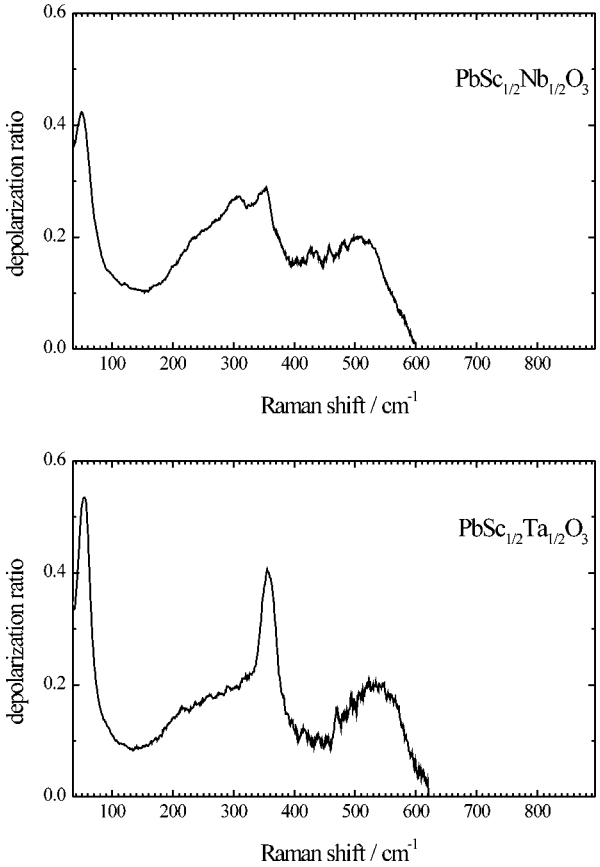

Figure 3. Depolarization ratios $I_\perp/I_{||}$ of $PbSc_{1/2}Nb_{1/2}O_3$ and $PbSc_{1/2}Ta_{1/2}O_3$ single crystals measured at 410 K, when the incident light is polarized along the cubic edge.

on modelling the modes in the paraelectric state and their dependence on small structural perturbations, i.e. short-range anisotropy. Firstly, we calculated the normal modes of a three-dimensionally polymerized $PbBO_3$ monomer and $Pb_2B_2O_6$ dimer (see figure 4) to clarify the effect of the doubling of the unit cell. Then, we analysed the mass and force constant effect on the mode frequencies of a $Pb_2B'B''O_6$ dimers. Finally, we investigated the mode dependence on various structural deviations from the ideal perovskite structure by calculating the normal modes of a $Pb_2B'B''O_6$ dimer when atomic shifts along the edge, the face diagonal or the body diagonal are assumed. The initial values of the force constants used in the calculations are given in table 5. These values were specified taking into account the interatomic distances, the valency and the coordination of the atoms. Nearly the same values of the B–O force constants have been used for $LiNbO_3$ and $LiTaO_3$ [33, 39]. Additional electrostatic local fields due to the presence of B cations of different valences were introduced for the oxygen atoms, which yielded a much better fit of the frequencies of the symmetrical stretching modes. Table 6 shows the calculated frequencies and the type of the eigenmodes for different cubic structural species, while the atomic displacements in the vibrational modes are plotted in figure 5. It is clearly seen from table 6 that the symmetrical B–O stretching near 820 cm^{-1} and the Pb-localized mode near 50 cm^{-1} can be observed in the Raman spectra only when the unit cell is doubled. Raman signals at such frequencies are always observed in the spectra of Pb-based

Table 5. Initial values of force constants used in the calculations.

Type of interaction		Value (N m^{-1})
B–O bond stretching,	B=Sc	160
	B=B″	185
O–B–O bond bending,	B=Sc	16
	B=B″	27
B–O–B bond bending		0.5
Pb–O bond stretching		15
O–Pb–O bond bending		1.1
Pb–O–Pb bond bending		1
B–O–Pb bond bending		1
B′–B″ Coulomb-type[a]		−75
Pb–Pb Coulomb-type[a]		−20

[a] Only for the nearest neighbours.

relaxors [13], which means that on a local scale doubling of the structural unit always occurs in these materials. The presence of B′–B″ pairs shifts O atoms along the cubic edge, thus stimulating the oxygen to be placed in $(0.25 + \delta x, 0, 0)$ position of space group $Fm\bar{3}m$. Our results support the conclusion of Siny *et al* [16] that the existence of nanosized clusters with $Fm\bar{3}m$ symmetry is a common feature of the relaxor structure. Additionally, we specified the wavenumber range of the E_g-mode and that of the F_g-mode related to the symmetrical BO_6 bending. The frequencies of the Raman-active modes A_g, E_g and F_{2g} as well as those of the silent modes F_{1g} and F_{2u} do not depend on the B-mass since the B cations do not participate in these modes (see figure 5). Therefore, these modes give rise to the mass-insensitive peaks P_1, P_2, P_5, P_7 and P_8, as discussed above. The infrared-active F_{1u} modes involves motions of B cations, therefore the mass-sensitive peaks P_3, P_4, P_6, P_9 and P_{10} should arise from F_{1u} modes which split into Raman-active A- and E-components under rhombohedral structural distortion. Using larger force constants for the tantalum–oxygen interactions than for the niobium–oxygen interaction, we successfully managed to fit most of the observed peak positions and the peaks P_1, P_2, P_3, P_5, P_6, P_{10} and P_{11} were easily assigned (see table 6). Hence, the broad band P_9 near 260 cm^{-1} for PSN and near 245 cm^{-1} for PST is generated from the F_{1u} (B-localized) and F_{1g} (BO_3 rotation) modes. The atom participants of these modes change when rhombohedral distortion occurs and the modes involve vibrations of both, the oxygen and the B-positioned atoms. Therefore, the Raman scattering near 820, 800, 540 and 50 cm^{-1} (P_1, P_2, P_5 and P_{11}) results from 'true' Raman-active modes, while the Raman scattering near 700, 430, 250 and 150 cm^{-1} (P_3, P_6, P_9 and P_{10}) is due to 'dirty' modes whose Raman activity is provoked by rhombohedral structural distortion. However, the origin of the peaks P_4, P_7 and P_8 remains obscure without detailed analysis of the mode dependence on the atomic deviations from the ideal perovskite structure.

It is well known that Pb^{2+} cations possess lone-pair electrons [25, 26, 40]. The existence of lone-pair states promotes electron–phonon coupling, thus leading to a lowering of the structure symmetry. Particularly, off-centre structural deviations are related to double-well atomic potential, i.e. to two-level systems. On the other hand, the mode F_{2u} is Raman active in absence of centre of inversion [32], i.e. this mode must be sensitive to local off-centred structural changes. In $PbSc_{1/2}B''_{1/2}O_3$ the Pb cations can easier form elongated lone pairs if they are linked with B cations of different valence along the body diagonal (see figure 6(a)). The atoms may shift along the body diagonal due to the different degree of covalency of B′–O and B″–O bonds and, in such a manner, lone pairs oriented along the body diagonal appear. Dynamical shifts of Pb and B cations in perovskite-type materials have already been detected by

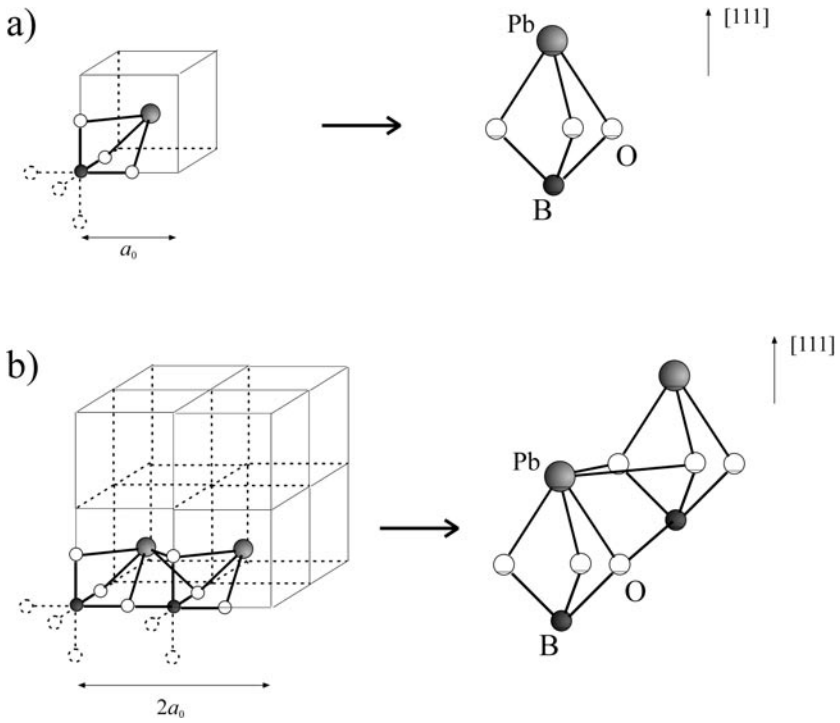

Figure 4. Structural units used for modelling the spectra of $PbSc_{1/2}B''_{1/2}O_3$, $B'' = Nb, Ta$. (a) $Pm\bar{3}m$ space group; (b) $Fm\bar{3}m$ space group.

Table 6. Calculated vibrational frequencies of paraelectric monomer and dimers.

Effect of doubling		B''-mass effect[a]		Effect of covalency[b]		
$PbNbO_3$	$Pb_2Nb_2O_6$	Pb_2ScNbO_6	Pb_2ScTaO_6	$Pb_2ScNbO_6^c$	$Pb_2ScTaO_6^c$	Type of vibration
—	810	793	793	810 (810)	823 (829)	A_{1g} sym B–O stretching
—	810	793	793	810 (796)	823 (805)	E_g sym B–O stretching
703	703	704	690	726 (700)	724 (700)	F_{1u} asym B–O stretching
—	531	485	485	527 (529)	535 (550)	F_{2g} sym O–B–O bending
440	440	413	406	446 (440)	439 (426)	F_{1u} asym O–B–O bending
409	409	379	379	406 (350–290)	411 (356–300)	F_{2u} BO_3 rotation
—	233	244	224	266 (260)	250 (245)	F_{1u} B-localized
—	230	230	230	230	230	F_{1g} BO_3 rotation
143	143	151	130	153 (152)	135 (146)	F_{1u} BO_3 translation
—	54	54	54	54 (50)	54 (53)	F_{2g} Pb-localized

[a] Equal niobium–oxygen and tantalum–oxygen interactions.
[b] $F(Nb–O) = 210$ N m^{-1}, $F(O–Nb–O) = 37$ N m^{-1}; $F(Ta–O) = 230$ N m^{-1}, $F(O–Ta–O) = 39$ N m^{-1}.
[c] In the parentheses are the experimental frequencies of the corresponding peaks.

nuclear magnetic resonance [41]. Also diffuse x-ray scattering along [111] has been observed in $PbSc_{1/2}B''_{1/2}O_3$ single crystals [30]. Thus, we propose that the Raman scattering 350 and 300 cm^{-1} is generated from the F_{2u} mode, whose Raman activity is caused by dynamical off-centred structural fluctuations due to electron–phonon coupling. The F_{2u} mode consists of O vibrations along the Pb–O bonds, i.e. it appears as a Pb–O bond-stretching mode in

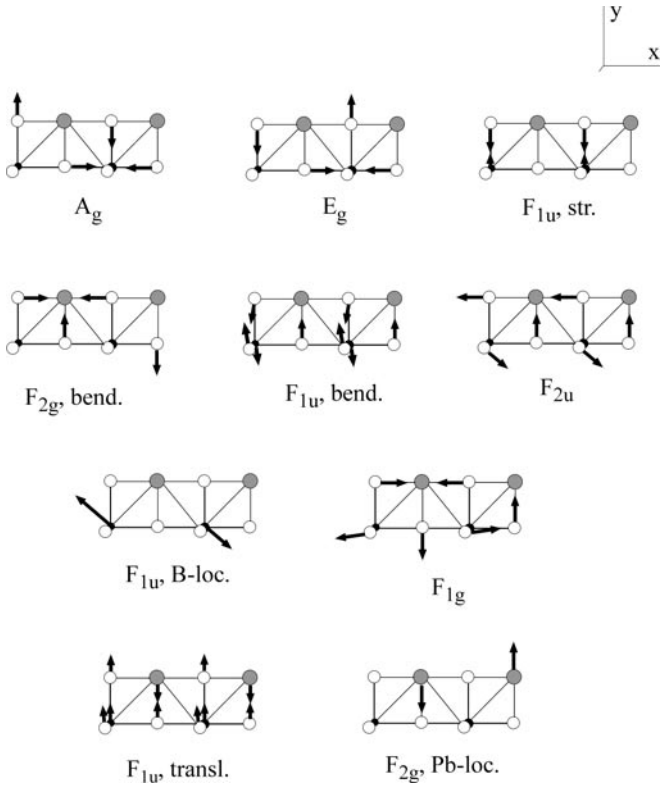

Figure 5. Atom vector displacements of the normal modes in the paraelectric state of $PbB'_{1/1}B''_{1/2}O_3$: grey circles, Pb atoms; black circles, B atoms; white circles, O atoms.

a lead–oxygen system. The difference in the intensity ratio I_{P_7}/I_{P_8} between PSN and PST can be understood by considering the modes in the two-dimensional Pb–O system which is perpendicular to the body diagonal (see figures 6(a) and (b)). If B′/B″ ordering exists, the orientations of the lone pairs within one Pb–O plane should be correlated. In this case all the Pb atoms will be shifted in the same direction with respect to the O atoms. If B′/B″ ordering is lacking, the lone pairs will be oriented up and down, i.e. the atomic shifts from the plane are not correlated. Figure 6(c) presents the spectrum profile of the Pb–O stretchings in the two-dimensional system. As seen, the intensity ratio between the higher-frequency and the lower-frequency peaks is larger in the case of correlated shifts, i.e. when chemical ordering exits. Indeed, the experimental intensity ratio I_{P_7}/I_{P_8} is higher in the PST spectrum, in which weak B′/B″ ordering was observed by single-crystal XRD, than that in the PSN spectrum, in which no compositional ordering was detected.

Furthermore we considered the effect of the atomic shifts in the normal modes of a $Pb_2ScB''O_6$ dimer. Deviations of the B atoms from the centre of BO_6 octahedra greatly increase the frequency of the asymmetrical O–B–O mode. When the B atoms are shifted along the body diagonal the frequency change is in the order of 150 cm^{-1}, regardless whether the B atoms are moved in the same, opposite or mutually perpendicular directions. Therefore, the peak P_4 results from off-centre distortion of BO_6 octahedra. Changes in the geometry of the BO_6 octahedra can also be realized by shifting the triad of oxygens shared between Pb and B (considering the O atoms placed in $(0.25 + \delta x, \delta z, \delta z)$ position). When the two oxygen

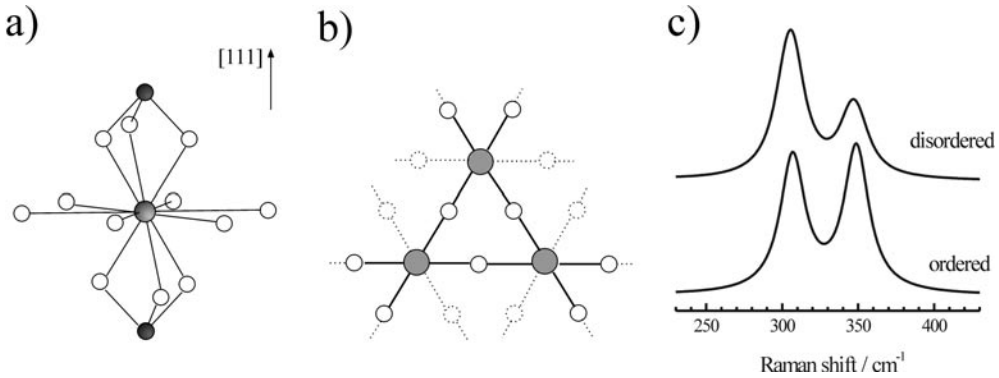

Figure 6. (a) Atomic surroundings of Pb in paraelectric $PbB'_2B''_{1/2}O_3$. (b) Top view of the Pb_3O_9 unit building a two-dimensional Pb–O system perpendicular to the body diagonal. (c) Calculated Raman scattering profile of ordered and disordered two-dimensional system with respect to the mutual deviation of the Pb atoms from the oxygen plane. The line intensities were broadened with Lorentzians of constant widths.

triads are shifted in opposite directions, the frequency of the asymmetrical O–B–O bending mode is not influenced, but when the triads are shifted in the same directions, the mode appears at much higher frequencies, as in the case of B deviations. Hence, the oxygen shifts split in frequency the Pb-localized F_{2g} mode near 50 cm^{-1}, whereas the B shifts do not affect this mode. The frequency splitting is due to the non-coplanarity of the Pb and O atoms in the plane perpendicular to the body diagonal, since the deviations of Pb atoms also split the mode. Thus, considering the Raman spectra of PSN and PST, particularly the temperature dependence of the P_4, P_6, P_{10} and P_{11} peaks, one can conclude that in PSN structural fluctuations consist predominantly of B atom deviations from the centre of BO_6 octahedra. The lowering of the temperature supports the deviations, thus leading to higher Raman scattering near 600 cm^{-1}. Also, on cooling the BO_3–Pb species harden due to the change in the B–O–Pb bond angle, thus increasing the frequency of the BO_3 translation mode. In PST the structural fluctuations consist mainly of mutual shifts of the O atoms with respect to the Pb atoms along to the body diagonal. The temperature decrease enhances the non-coplanarity of the Pb–O sheets perpendicular to the body diagonal. Hence, the difference in the preferential structural fluctuations determines different mechanisms of the ferroelectric phase transition in the two materials studied: (i) plane correlation of the orientations of the lone pairs of Pb and then correlation between layers (as in the case of PST) or (ii) BO_3 shift with respect to Pb without a preferred correlation direction (as in the case of PSN). The mechanisms involved should depend on both the B-mass difference and the degree of chemical ordering.

4. Conclusions

The appearance of Raman peaks arising from symmetrical B–O stretching modes in the spectra of $PbSc_{1/2}B''_{1/2}O_3$ shows that on a local scale of a few unit cells doubling of the structural unit is always possible. The shift of the oxygen atoms along the cubic edge is promoted by the presence of B′–O–B″ linkages.

The existence of two Raman signals originating from the F_{2u} mode shows that electron–phonon coupling occurs in $PbSc_{1/2}B''_{1/2}O_3$, thus leading to dynamical off-centre-symmetrical structural fluctuations. The structural perturbation consists of the non-coplanarity of the Pb and O atoms in the planes perpendicular to the body diagonal and deviations of B cations

from the centre of BO_6 octahedra. The intensity ratio of the two peaks is sensitive to the degree of correlation of the lone pairs of the Pb atoms within the Pb–O planes, which is related to the degree of compositional B′/B″ ordering. The intensity ratio between the higher- to lower-frequency peaks is larger for regions with higher degrees of ordering.

The temperature dependence of the peaks arising from the asymmetrical O–B–O bending, the BO_3 translation and the Pb-localized modes shows that on cooling different structural changes dominate in the two materials studied. In PSN the temperature decrease stabilizes and enhances the off-centre deviations of the B cations. This can be seen from the increase in the intensity of the peak near 600 cm^{-1} and the frequency shift to higher energies of the peak near 150 cm^{-1}. In PST the temperature decrease stabilizes the non-coplanarity of the Pb and O atoms in the planes perpendicular to the body diagonal and enhances the correlation between the electronic lone pairs of Pb.

Acknowledgments

BM is indebted to the Alexander von Humboldt Stiftung for a research grant. Financial support from the Bundesministerium für Bildung und Forschung is gratefully acknowledged. The authors thank Dr Klaska for help with the XRD data.

References

[1] Bhalla A S, Guo R and Roy R 2000 *Mater. Res. Innovat.* **4** 3–26
[2] Groves P 1985 *J. Phys. C: Solid State Phys.* **18** L1073–8
[3] Kang Z C, Caranoni C, Siny I, Nihoul G and Boulesteix C 1990 *J. Solid State Chem.* **87** 308–20
[4] Knight K S and Baba-Kishi K Z 1995 *Ferroelectrics* **173** 341–9
[5] Malibert C, Dkhil B, Kiat J M, Durand D, Bérar J F and Spasojevic-de Biré A 1997 *J. Phys.: Condens. Matter* **9** 7485–500
[6] Perrin C, Menguy N, Suard E, Muller Ch, Caranoni C and Stepanov A 2000 *J. Phys.: Condens. Matter* **12** 7523–39
[7] Dmowski W, Akbas M K, Davies P K and Egami T 2000 *J. Phys. Chem. Solids* **61** 229–37
[8] Takesue N, Fujii Y, Ichihara M and Chen H 1999 *Phys. Rev. Lett.* **82** 3709–12
[9] Reaney M, Petzelt J, Voitsekhovskii V V, Chu F and Setter N 1994 *J. Appl. Phys.* **76** 2086–92
[10] Petzelt J, Buixaderas E and Pronin A V 1998 *Mater. Sci. Eng.* B **55** 86–94
[11] Bismayer U, Devarajan V and Groves P 1989 *J. Phys.: Condens. Matter* **1** 6977–86
[12] Idink H and White W 1994 *J. Appl. Phys.* **76** 1789–93
[13] Husson E 1998 *Key Eng. Mater.* **155–6** 1–40 and references therein
[14] Rogacheva E A 2000 *Physica B* **291** 359–67
[15] Jiang F, Kojima S, Zhao C and Feng C 2000 *J. Appl. Phys.* **88** 3608–12
[16] Siny I G, Katiyar R S and Bhalla A S 2000 *Ferrolectrics Rev.* **2** 51–113
[17] Kreisel J, Glazer A M, Bouvier P and Lucazeau G 2001 *Phys. Rev.* B **63** 174106–16
[18] Blinc R, Gregorovič A, Zalar B, Pirc R, Laguta V V and Glinchuk M D 2001 *J. Appl. Phys.* **89** 1349–54
[19] Randall C A, Barber D J, Whatmore R W and Groves P 1986 *J. Mater. Sci.* **21** 4456–62
[20] Bursill L A, Julin P, Hua Q and Setter N 1995 *Physica B* **205** 305–26
[21] Lemmens H, Richard O, Van Tendeloo G and Bismayer U 1999 *J. Electron-Microsc.* **48** 843–7
[22] Abplanalp M, Barošová D, Bridenbaugh P, Erhart J, Fousek J, Günter P, Nosek J and Šulc M 2001 *Solid State Commun.* **119** 7–12
[23] Setter N and Cross L E 1980 *J. Appl. Phys.* **51** 4356–60
[24] Chu F, Setter N and Tagantsev A K 1993 *J. Appl. Phys.* **74** 5129–34
[25] Chen I-W, Li P and Wang Y 1996 *J. Phys. Chem. Solids* **57** 1525–36
[26] Burton B P 2000 *J. Phys. Chem. Solids* **61** 327–33
[27] Davies P K and Akbas M A 2000 *J. Phys. Chem. Solids* **61** 159–66
[28] Stenger C G F and Burggaaf A J 1980 *Phys. Status Solidi* a **61** 275–85
[29] Shannon R D 1976 *Acta Crystallogr.* A **32** 751–67

[30] Pietraszko A, Wolcyrz M, Hilczer B and Caranoni C 2001 *20th European Crystallographic Meeting ECM20, (Aug. 2001) (Book of Abstracts)* ed K Stadnicker and W Nitek p 187
[31] Dawber M, Ríos S, Scott J F, Qi Zhang and Whatmore R W 2001 *Fundamental Physics of Ferroelectrics 2001 (AIP Conf. Proc. CP582)* ed H Krakauer (New York: AIP) p 1
[32] Rousseau D L, Bauman R P and Porto S P S 1981 *J. Raman Spectrosc.* **10** 253–90
[33] Repelin Y, Husson E, Bennani F and Proust C 1999 *J. Phys. Chem. Solids* **60** 819–25
[34] Mihailova B, Zotov N, Marinov M, Nikolov J and Konstantinov L 1994 *J. Non-Cryst. Solids* **168** 265–74
[35] Mihailova B, Marinov M and Konstantinov L 1994 *J. Non-Cryst. Solids* **176** 127–32
[36] Furukawa T, Fox K and White W 1981 *J. Chem. Phys.* **75** 3226–37
[37] Lippincott E and Stutman J 1964 *J. Phys. Chem.* **68** 2926–40
[38] Bell R J 1976 *Meth. Comput. Phys.* **15** 215–76
[39] Mihailova B, Savatinova I, Savova I and Konstantinov L 2000 *Solid State Commun.* **116** 11–15
[40] Cohen R E 1992 *Nature* **358** 136–8
[41] Rod S, Borsa F and van der Klink J J 1988 *Phys. Rev.* B **39** 2267–72